

An adaptive weighting algorithm for accurate radio tomographic image in the environment with multipath and WiFi interference

International Journal of Distributed
Sensor Networks
2017, Vol. 13(1)
© The Author(s) 2017
DOI: 10.1177/1550147716683826
journals.sagepub.com/home/ijdsn


Manyi Wang¹, Zhonglei Wang², Xiongzhu Bu¹ and Enjie Ding³

Abstract

Radio frequency device-free localization based on wireless sensor network has proved its feasibility in buildings. With this technique, a target can be located relying on the changes of received signal strengths caused by the moving object. However, the accuracy of many such systems deteriorates seriously in the environment with WiFi and the multipath interference. State-of-the-art methods do not efficiently solve the WiFi and multipath interference problems at the same time. In this article, we propose and evaluate an adaptive weighting radio tomography image algorithm to improve the accuracy of radio frequency device-free localization in the environment with multipath and different intensity of WiFi interference. Field experiments prove that our approach outperforms the state-of-the-art radio frequency device-free localization systems in the environment with multipath and WiFi interference.

Keywords

Radio tomographic image, multipath, WiFi interference, adaptive weighting, sensor network

Date received: 23 March 2016; accepted: 18 September 2016

Academic Editor: Shinsuke Hara

Introduction

In recent years, localization awareness applications have been attracting more and more attentions. Global positioning system (GPS) is used for outdoor environment navigation. Radio frequency identification (RFID) and radio frequency (RF) are adopted for indoor localization and asset tracking. All the aforementioned techniques belong to the active localization, which can only work with the cooperation of the objects, carrying the electronic device.¹⁻³ However, these techniques cannot be used in scenarios where the objects do not wish to take any electronic device (e.g. terrorist attack, criminal behavior, and patients in the hospital). For this reason, Radio Frequency Device-free Localization (RFDFL) is adopted to locate the object without attaching any electronic tags.⁴⁻⁶ This technique has proved its feasibility in fall detection,⁷ roadside surveillance,⁸ ambient

assisted living⁹ non-invasive breathing monitoring,¹⁰ residential monitoring,¹¹ and multi-object localization.¹² Compared with the traditional security schemes (i.e. ground patrols and aerial surveillance from manned or unmanned aircraft), RFDFL can be used for illegal abroad crossings surveillance in a resource-intensive and a low-cost way.⁸

¹School of Mechanical Engineering, Nanjing University of Science and Technology, Nanjing, China

²Karlsruhe Institute of Technology (KIT), Karlsruhe, Germany

³Internet of Things Research Center, China University of Mining and Technology, Xuzhou, China

Corresponding author:

Enjie Ding, Internet of Things Research Center, China University of Mining and Technology, Xuzhou, Jiangsu 221116, China.
Email: enjied@cumt.edu.cn



Compared with other device-free localization (DFL), RFDFL can be utilized to locate/track objects in the environment with obstruction and without illumination. In addition, this technique has no invasion of privacy. Compared with the infrared system and radar system, it can monitor larger area. What's more, it is much cheaper than the ultra wideband system.^{4,5,13} The essence of RFDFL is that wireless sensor nodes are deployed around the perimeter of the monitored area, each sensor takes turns to send packets to all other sensors at a high frequency. The received signal strength (RSS) of the communication link will be attenuated because of the obstruction of the object in the monitored area. By observing attenuations of all links, RFDFL is able to extract the location of the object by analyzing the changes in the RF propagation field of the located area.⁴

For RFDFL systems, there are three widely utilized methods including the fingerprint method,^{6,13} the Bayesian inference approaches (e.g. Sequential Monte Carlo method),⁵ and the imaging approach referred to as the radio tomographic imaging (RTI).^{4,14} For the fingerprint method, it needs an offline phase, which is used to collect the radio maps when the object stands on different predetermined locations, and then the system maps the estimated location to one of the trained locations based on the changes of the communication link RSS, the closest matching is utilized to refer to as the object's location during the online phase. In order to achieve a stable accuracy, the offline phase should be repeated when the radio transmission environment changes, which is really time- and manpower-consuming. The Bayesian inference approach relies on recursive computation of the large number of particles, which is not applicable to real-time localization. In RTI, a radio tomography image inferring the object's location can be obtained by analyzing the attenuation of all radio links in the monitored area. It has been proved that it is an efficient way for localization through the wall, monitor or locate a breathing in the residential area.

Radio signal (2.4 GHz) is more sensitive than any other frequency signals.¹⁵ The reason is that the resonant frequency 2.4 GHz frequency and water are the same and more than 70% of the human body is composed of water. Thus, 2.4 GHz radio signal is more sensitive than any other frequency signals.¹⁵ The state-of-the-art RFDFL systems^{4,5,14,16,17} extensively use 2.4 GHz (IEEE 802.15.4 compliant) sensor nodes to locate the object. Consequently, the problems at hand are twofold. First, how to guarantee the accuracy of RFDFL localization under WiFi interference. WiFi networks share the same operating frequency with IEEE 802.15.4 sensor network. The burst and concurrent communication of WiFi networks lead to severe interference to 2.4 GHz sensor network, resulting in serious packet drops.^{18,19} If packet drops, RFDFL

cannot obtain the real-time RSS measurement of radio links. Instead, it uses the previous RSS measurement to calculate the object localization, which introduces a large location error.²⁰ However, state-of-the-art methods cannot solve this problem. Second, multipath interference also degrades the accuracy of RFDFL severely. The state-of-the-art RFDFL assumes that the obstruction of the object attenuates the RSS of the radio link. However, the RSS at the receiver is determined by the summation of radio waves phasor from multipath. Therefore, RSS variance introduced by a human or an object is probably to be increased, reduced, or constant. This is highly related to the transmission RF. For a given link, if the chosen RF is not the one attenuated by the object, it will cause large accuracy errors. Although there is research work presenting solution to this problem, it is still not sufficiently settled.

In this article, we propose a novel adaptive channel weight model to solve these problems at the same time. First, we obtain the fade level of each measurement channel for every communication link during the calibration time. Second, the real-time packet drop rate (PDR) of the measurement channels can be calculated with an online observation window. Then, we propose an adaptive channel weight model to obtain the adaptive weight for each measurement channel, by fusing the two aforementioned factors. Due to considering both the WiFi interference and multipath interference, we benefit from the adaptive channel weight model in the environment with multipath and WiFi interference.

The rest of the article is organized as follows: section "Related work" discusses the related work. In section "Adaptive weighting RTI," shadowing-based RTI is introduced. The influence factors to the accuracy of RFDFL and our new adaptive weight model are presented in section "Experiments." Section "Experiments" describes the experiment setup and shows our experimental results. Finally, the article is concluded in section "Conclusion."

Related work

In this section, we review the previous works related to RFDFL methods and the accuracy enhancement of RFDFL with wireless sensor network. The fingerprint model^{6,21,22} is composed of the offline phase and the online phase. During the offline phase, a radio map is generated for predetermined location of the target and stored in the database. During the online localization, the obtained radio map is compared with the stored radio maps. The closest matching is used to infer the target's location. The scalability of this method is very limited. If the topology of the WiFi network is changed, the offline phase must repeat, which is a very time-consuming process. Chen et al.⁵ proposed to use

Sequential Monte Carlo algorithm for DFL. This method suffers from intensive computation and is not suitable for real-time localization. In 2010, Wilson and Patwari⁴ introduced the RTI method for DFL,^{4,16,23–25} which is more effective. They localize the target in the RF propagation area using attenuation of RSS values caused by the target. However, all RTI methods are based on 2.4 GHz IEEE 802.15.4 sensor network and their accuracy is not only highly influenced by multipath interference but also WiFi interference, which are not well addressed in the previous work. Kaltiokallio et al.²³ proposed to use the multi-channel mechanism to stand up to multipath interference in the indoor environment. In this method, all sensor nodes operate on multi-channel. Each communication link ranks the channels from anti-fade to deep fade based on the fade level. The measurement of the top m (set by users) anti-fade channels were used for RTI localization. Their later work in Bocca et al.¹² weights all the measurement channels based on their fade level to improve the localization accuracy. However, WiFi interference is not considered in both of the works. Anti-fade channels may suffer from severe PDR and lose extreme important localization information because of the WiFi interference. In Zhao and Patwari,²⁴ although subspace decomposition method is adopted to improve the localization accuracy by reducing the effect of the environment noise (e.g. vibration of tree branches, wind blowing) on the RSS value, multipath and WiFi interference are still not addressed. Their later work in Zhao et al.¹⁶ presents a method to improve the localization accuracy by calculating kernel distance. With this method, the kernel distance between a long-term histogram and a short-term histogram is adopted to obtain the temporal RSS changes caused by the target. However, they only use channel 26 of 2.4 GHz sensor network for RFDL which is assumed not to be interfered by WiFi network. To improve accuracy, a multi-scale spatial weight model is proposed in Kaltioallio et al.,²⁵ where different spatial weights are assigned to each link based on the fade level. However, deterioration of localization accuracy caused by WiFi interference is not taken into consideration. Similarly, dual-band sensor network only solves the problem of WiFi interference, the accuracy deterioration caused by multipath is still not efficiently solved.²⁰

Adaptive weighting RTI

Characteristics of the RSS in the WiFi environment

In order to clarify the effect of the WiFi interference on the localization accuracy and determine the main reason leading to deterioration of the localization accuracy, we extract the following data under different intensity of WiFi interference during the experiment:

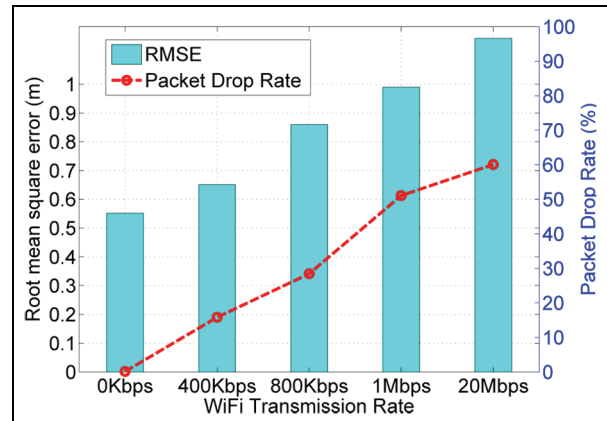


Figure 1. The changes of PDR and accuracy of RFDL system working on IEEE 802.15.4, with WiFi interference increasing.

PDR of each communication link working on channel 18, and the localization accuracy of RFDL operating on channel 18 as shown in Figure 10. Clearly, we can see that the PDR and the accuracy of RFDL are both deteriorated and have the same trend. In fact, we also obtain the similar experiment results with channel 26. For simplicity, only the results using channel 18 are shown here. The experimental setup is described in detail in section “Experimental setup.”

In RFDL systems, the RSS variance caused by obstruction of the object is used to do localization. The one and only reasonable explanation to deterioration of RFDL accuracy is that the variance of RSS is not aroused by the object, but the WiFi interference. As shown in Figure 1, we use different WiFi transmission volume to indicate diverse intensities of WiFi interference.²⁶ Clearly, the accuracy of RFDL becomes worse with the increase in the WiFi interference, as shown in Figure 1.

Intuitively, accuracy of RFDL has tight relationship with PDR because PDR holds the same trend as the accuracy of RFDL under WiFi interference. To further verify this, the real-time sampling RSS values and their corresponding variance are shown in Figure 2. From this figure, it can be seen that WiFi interference almost has no obvious influence on changes of RSS itself. Based on the aforementioned analysis, PDR is the main reason to decrease the accuracy of RFDL. In other words, if the packets are dropped, RFDL cannot obtain the up-to-date RSS values, which comprise the location information of the object at this moment. Instead of using the up-to-date RSS values, the previous RSS measurements are used to extract the location of the object by RFDL. Hence, the main reason causing the deterioration of RFDL accuracy is not the variance of RSS value, but rather PDR caused by WiFi interference. So, it is reasonable for us to utilize PDR of IEEE 802.15.4 communication

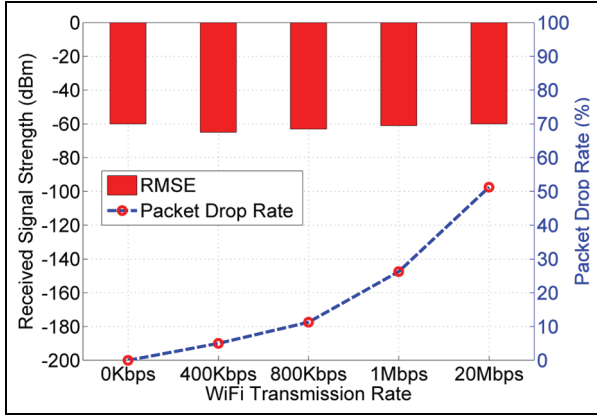


Figure 2. RSS and PDR of 2.4 GHz communication link working on channel 18 under different intensity of WiFi interference.

link to represent the intensity of WiFi interference and adopt the criterion of PDR to choose the most robust communication channel for each of the communication link.

Characteristics of the RSS in multipath environment

Fade level²³ is used to depict the relationship between steady-state, narrow-band fading and variance of RSS introduced by human body's obstruction on the radio communication link. The metric of the fade level categorizes the communication channels of a given link into two extremes: deep fade channel and anti-fade channel. For the link operating on the deep fade channel, the RSS, on average, increases when the object obstructs the link. Additionally, the presence of the object, which is even far away from the link, will result in obvious RSS changes in deep fade channel (e.g. channel 15 as shown in Figure 3). In contrast, the RSS value of anti-fade channel, on average, attenuates when the object obstructs the link. In addition, the RSS of anti-fade channel will not change until the target is in proximity to the link (e.g. channel 11 and channel 18 as shown in Figure 3). Because of more precise position of the human are contained in the anti-fade channel, thus, we can achieve more accurate result, if all communication links in RFDL adopt their corresponding anti-fade channel. Mathematically, the fade level can be expressed as follows²³

$$\gamma_{i,c} = \tilde{P}_c - L_{i,c} - S_{i,c} + F_{i,c} - n_{i,c} \quad (1)$$

where $\gamma_{i,c}$ is the RSS measurement of the i th link on channel c , \tilde{P}_c is the transmission power, $L_{i,c}$ is the large scale path loss, $S_{i,c}$ is the shadowing loss caused by an object, $F_{i,c}$ is the fade level,²⁷ and $n_{i,c}$ is the measurement noise.

Then, the fade level can be expressed as

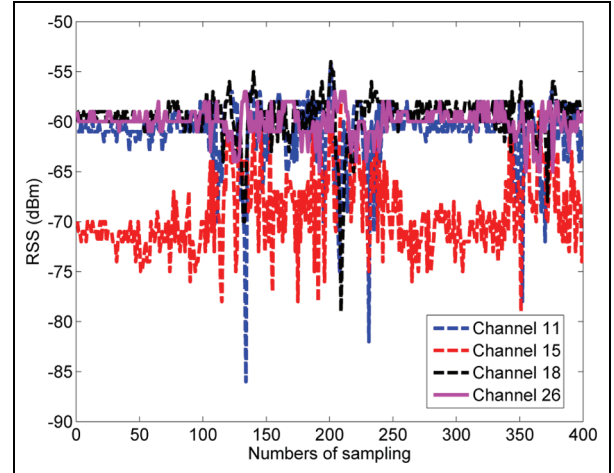


Figure 3. RSS of 2.4 GHz communication link operating on different channels in indoor environment (with a person existence).

$$F_{i,c} = \gamma_{i,c} - \tilde{P}_c + \underbrace{L_{i,c} + S_{i,c}} + n_{i,c} \quad (2)$$

For IEEE 802.15.4-complaint sensor network, it has 16 frequency channels spanning over 80 MHz band, with only 5 MHz frequency interval.²⁸ Thus, the large scale path loss $L_{i,c}$ and shadowing loss $S_{i,c}$ (as shown in Formula (3)) change very slowly with the center frequency. Based on this, we assume that $L_{i,c}$ and $S_{i,c}$ almost have no relationship with frequency channel c . Then, Formula (2) can be rewritten as

$$F_{i,c} \approx \gamma_{i,c} - \tilde{P}_c + n_{i,c} \quad (3)$$

In practice, because $n_{i,c}$, $L_{i,c}$, and $S_{i,c}$ are not known, it is difficult to obtain the fade level on each channel from the measurement, precisely. We perform an initial phase (no human in the monitored area) and measure the average RSS, $\bar{\gamma}_{i,c}$. The minimum $\min_c \bar{\gamma}_{i,c}$ of the link i on channel c is adopted as the reference to calculate the fade level of link i . Thus, instead of Formula (3), we use Formula (4) to calculate the fade level. Experimental results proved its feasibility in section "Experiments"

$$F_{i,c} = \bar{\gamma}_{i,c} - \min_c \bar{\gamma}_{i,c} \quad (4)$$

where for the link i , the channel c_2 is in a deeper fade, if $F_{i,c_1} > F_{i,c_2}$. In addition, for every communication link, $F_{i,c} \geq 0$ and $F_{i,c} = 0$ for one channel.

Based on the aforementioned analysis of fade level, we know that the anti-fade channels are more informative than the deep fade channels for RFDL in the environment with multipath interference because of its restrictive sensitivity area to human body obstruction. However, all IEEE 802.15.4 channels (channels 11–26)

are overlapped by IEEE 802.11 WiFi networks. For RTI systems, even though most anti-fade channels are selected for localization during the calibration time, they have quite high probability interfered by WiFi signals operating on the adjacent channels, which results in severe PDR of the most anti-fade channel and location information loss, which lead to deteriorative localization accuracy.

Adaptive channel weight model

WiFi networks share the same operating frequency with IEEE 802.15.4 sensor network. The burst or concurrent communication of WiFi networks lead to severe interference to 2.4 GHz sensor network resulting in serious packets drops, which causes the RFDFL cannot obtain the up-to-date measurement of communication link, and results in the deterioration of localization accuracy of RFDFL.

In addition, multipath is another severe problem, which should be taken into consideration. The state-of-the-art RFDFL assumes that the obstruction of the human body attenuates the RSS of radio link. However, RSS variance introduced by the human in the multipath environment is probable to increased, reduced, or constant. This is highly related to the transmission RF. For a given link, if the chosen radio channel is not the one attenuated by the object, it will cause large accuracy error.

The state of the art does not settle the aforementioned problems efficiently at the same time. Considering both the WiFi interference and multipath interference simultaneously, we propose a combined weight model (seen in Formula (6)) to assign different weights to each channel according to the intensity of multipath and WiFi interference. Specifically, for the communication link i , working on n different channels ($c = [ch_1, \dots, ch_i, \dots, ch_n]$), the channel ch_i holds the maximum weight when it owns the lowest $PDR_{i,c}$ and the largest $F_{i,c}$ (suffering from the lowest multipath and WiFi interference), compared with the other $(n - 1)$ channels. In addition, compared with the state of the art,²³ the measurement information from all other channels are also taken into consideration in our model, which also contributes to the localization accuracy. Mathematically, it can be expressed as

$$\gamma_{i,c}(n) = \frac{1}{\sum_{c \in K} W_{i,c}} \sum_{c \in K} W_{i,c} |\Delta\gamma_{i,c}(n)| \quad (5)$$

where $W_{i,c}$ is the weight of the c th channel for the i th communication link as shown in equation (6)

$$W_{i,c} = \frac{F_{i,c}}{\varepsilon + PDR_{i,c}} \quad (6)$$

where $F_{i,c}$ is the fade level of the i th communication link operating on channel c , K is the predetermined channel set of the communication link. ε in (equation (6)) is used to avoid division by zero, $PDR_{i,c}$ is the packet drop rate of the i th communication link working on channel c

$$\Delta\gamma_{i,c}(n) = \bar{\gamma}_{i,c} - \gamma_{i,c}(n) \quad (7)$$

Here, $\Delta\gamma_{i,c}(n)$ is the RSS change of the i th communication link at time n , compared with the calibration value. We use pseudo-code to explain more concretely the process of the adaptive channel weight model as shown in algorithm 1.

Measurement model of the RTI

In RTI, 2.4 GHz sensor nodes are deployed around the monitored area and form an observation area. Logically, RTI splits the monitored area into small voxels. For a given link, the change of RSS is assumed to be the accumulation of all the small voxels of the monitored area. Some voxels contribute to the link, whereas others do not. Mathematically, it can be expressed as

$$\Delta\gamma_i = \sum_{j=1}^N w_{ij} \Delta x_i + n_i \quad (8)$$

where Δx_i is attenuation caused by voxel i , n_i is the measurement noise of link i , N is the number of voxels, $\Delta\gamma_i$ is the RSS change of the link i , and w_{ij} is the weight of voxel j for link i . We use an ellipse model^{4,14,23} to calculate, how each voxel affects each link. As shown in Figure 4, only voxels located in the ellipse can affect the communication link i . For example, according to the ellipse model, a voxel j at the position of C_j contributes to the RSS change of the link i with the weight w_{ij} , which is inversely proportional to the area of the ellipse

$$w_{ij} = \frac{1}{S_i} \begin{cases} 1, & \text{if } d_{ij}^t(x_j) + d_{ij}^r(x_j) < d_{ij}^t + \lambda \\ 0, & \text{otherwise} \end{cases} \quad (9)$$

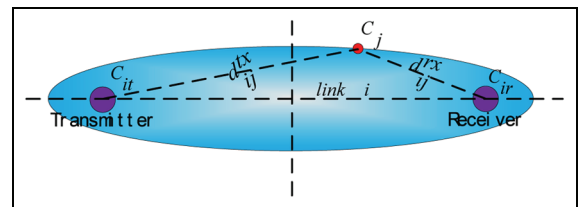


Figure 4. Weight model.

Algorithm 1: Adaptive Channel Weight Model**Initialize:**

All sensor nodes operate on the predetermined channel list C .

Input:

The coordinators of the sensor nodes $(x_m, y_m)_{m=1,2,\dots}$.

Measuring the RSS of all communication links working on channel list $C = [ch_1, ch_2, \dots, ch_K]$.

Output:

The estimated location of the person in the monitored area: (x_t, y_t) .

Calculate:

Calculating the projection matrix $\mathbf{\Pi} = (\mathbf{W}^T \mathbf{W} + \delta_N^2 \mathbf{C}_x^{-1}) \mathbf{W}^T$.

Calculating the fade level of each measurement channel for every communication link $F_{i,c} = \bar{\gamma}_{i,c} - \min_c \bar{\gamma}_{i,c}$.

while: (1) do

1. obtaining the $PDR_{i,c}$; /* the observation length is L^* */

2. calculating the combination weight: $W_{i,c} = F_{i,c} / (\varepsilon + PDR_{i,c})$;

3. calculating the RSS change of every communication link: $\gamma_{i,c}(n) = 1 / \sum_{c \in K} W_{i,c} * (\sum_{c \in K} W_{i,c} |\Delta \gamma_{i,c}(n)|)$;

4. obtaining the RSS value of every communication link at time n : $\gamma = [\gamma_1(n), \gamma_2(n), \dots, \gamma_N(n)]$; /* N is the number of the communication link */

5. calculating the radio tomography image: $\hat{\mathbf{x}} = \mathbf{\Pi} \gamma$;

6. obtaining the location of the person: $(x_t, y_t) = \arg \max_N(\hat{\mathbf{x}})$. /* N is the number of the grid */

End

where S_i is the area of the ellipse, $d_{ij}^t x_j = \|\mathbf{C}_{it} - \mathbf{C}_j\|$, $d_{ij}^r x_j = \|\mathbf{C}_{ir} - \mathbf{C}_j\|$, $d_{ij}^{rr} = \|\mathbf{C}_{it} - \mathbf{C}_{ir}\|$, \mathbf{C}_{it} is the coordinator of transmitter, \mathbf{C}_{ir} is the coordinator of receiver, and λ is the parameter used to adjust the width of the ellipse.

Mathematically, if we consider all the communication links, RSS changes of all the communication links in the radio propagation field can be expressed as ^{4,29,30}

$$\Delta \gamma = \mathbf{W} \Delta \mathbf{x} + \mathbf{n} \quad (10)$$

where $\Delta \gamma$ is an $L \times 1$ vector representing the RSS change of all communication links. \mathbf{W} is the weight matrix with size of $L \times N$. \mathbf{n} is the measurement noise of all communication links with size of $L \times 1$.

RTI estimates the location of the object according to the value of the voxel. The coordinator of the voxel with maximum value in $\Delta \mathbf{x}$ is referred to as the location of the object. Due to the measurement noise of \mathbf{n} , the same RSS change $\Delta \gamma$ results in multiple $\Delta \mathbf{x}$, here we use a regularized least-square approach to solve the ill-posed inverse problem. Mathematically, it is denoted by the following equations

$$\hat{\mathbf{x}} = \mathbf{\Pi} \Delta \gamma \quad (11)$$

where

$$\mathbf{\Pi} = (\mathbf{W}^T \mathbf{W} + \delta_N^2 \mathbf{C}_x^{-1}) \mathbf{W}^T \quad (12)$$

in which δ_N^2 is the variance of the environment noise, and \mathbf{C}_x is a covariance matrix representing by an exponential spatial decay

$$[\mathbf{C}_x]_{jk} = \delta_x^2 e^{-d_{jk}/\delta_c} \quad (13)$$

Table 1. RTI parameters.

Parameter	Value	Description
δ_N^2	1	Variance of environment noise
δ_x^2	0.5	Variance of pixel attenuation
δ_c	3	Correlation used to smooth the image
λ	0.25	Half minor axis length (m)
p	0.2	Pixel width (m)
ε	0.01	Avoid division by zero in seconds.

RTI: radio tomographic imaging.

where δ_x^2 is variance of the voxel attenuation, δ_c is the voxels' correlation distance, and d_{jk} is the Euclidean distance between voxel j and voxel k . The vector $\mathbf{\Pi}$ is calculated only once at the beginning of the localization process, thus RTI needs only $L \times N$ operations to calculate the $\hat{\mathbf{x}}$. So it can do the calculation in real time. The aforementioned parameters and their values are listed in Table 1 in the adaptive weighting RTI algorithm. Note that we could tune these parameters for a particular experiment to obtain higher localization accuracy.

Experiments

Experimental setup

In order to evaluate the effect of the adaptive weighting RTI algorithm, we implemented the experiments in the Internet of Things (IOT) exhibition hall of China University of Mining and Technology (CUMT) during the midnight, when there is almost no WiFi interference.

Figure 5(a) shows a picture of the experiment environment. A total of 20 USB dongles with IDs, from 0 to 19, are distributed along the perimeter of a

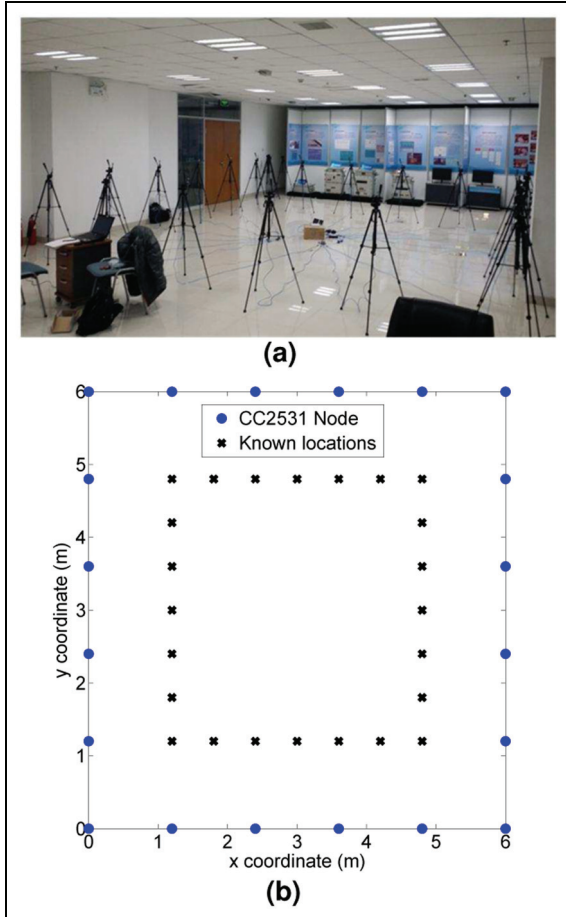


Figure 5. Experiment layout and environment: (a) environment and (b) layout of the experiment, distance between two node is set to 1.2 m.

rectangular area as shown in Figure 5(b). Each USB dongles (seen in Figure 6) is put on a tripod at a height of 1.2 m, as given in Figure 5(a).

At the beginning of the experiments, 40-s calibration time is needed to obtain the mean RSS value on each communication link without any person in the monitoring area. During the experiments, a person stands at 24 pre-marked locations as shown in Figure 5(b). Figure 5(b) shows the distribution of 20 USB dongles operating on 2.4 GHz band³¹ with IDs from 0 to 19. The USB dongles are put on a tripod, as shown in Figure 6. Figure 5(a) gives a picture of the experimental environment.

Each USB dongle working at 2.4 GHz is composed of a CC2531 microchip. Their transmission power is 4.5 dBm. They all run the multi-spin communication protocol⁴ for communication. The procedure of Spin is that all nodes in network take turns to transmit data according to their node IDs, which is programmed beforehand. At any particular time, only one node is transmitting while the others are listening. When a packet is dropped or a node fails to transmit, a timer

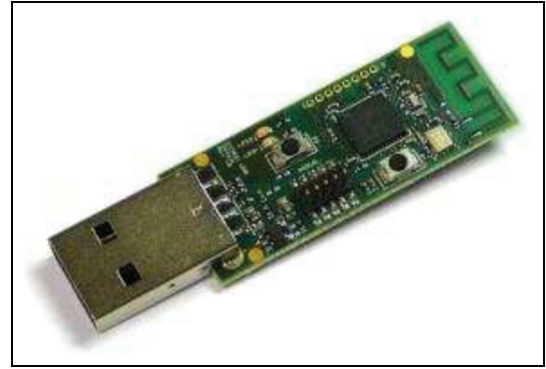


Figure 6. Wireless sensor node (CC2531 USB Dongle).

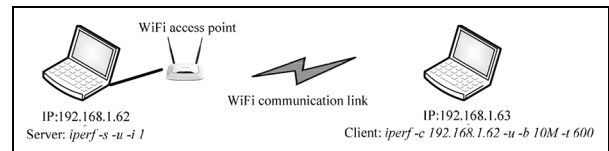


Figure 7. The topology of WiFi interference network.

will fire to make sure that the next node moves on. At the end of each communication cycle, all nodes switch synchronously to the next channel. The available channels are pre-defined. Channels 11, 18, 21, and 26 are used in our experiment.

To generate different intensities of WiFi interference, we followed the same approach as in Liang et al.¹⁹ We used two laptops and one WiFi access point to build a WiFi network. One laptop acted as a server, while the other one used the iperf tool³² to produce different intensities of WiFi interference by requesting different transmission rates from the server, as shown in Figure 7.

Results and discussion

In this subsection, we focus on evaluating the performance of the adaptive weighting RTI algorithm using the aforementioned experimental setup. The experimental results show that our adaptive weighting RTI algorithm outperforms the state of the art.

In the following experiments, the intensity of WiFi interference was set to 0 kbps, 800 kbps, 1 Mbps, 2 Mbps, 4 Mbps, 6 Mbps, and 10 Mbps, respectively. As shown in Figure 8, PDR of each communication link (working on channel 18) between the 1st node and the others (e.g. L_1, L_2, \dots, L_{19}), increased with increasing of the WiFi interference. For example, PDRs of the communication link L_1 was almost 0 in the environment without WiFi interference, and became the worst (63.6%) under 10 Mbps WiFi interference, the other

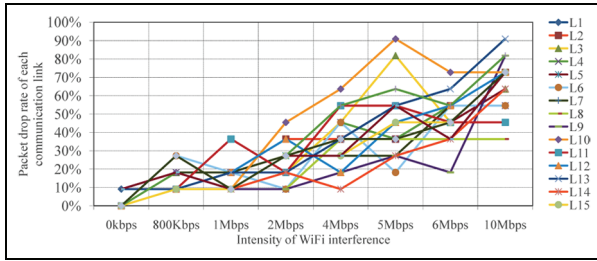


Figure 8. Packet drop rate of each communication link (on channel 18) between the l th node and the others under different WiFi interference.

communication links follow the same trend. In addition, the PDR of each communication link is not the same as each other under the same intensity of WiFi interference, this is because the distance between the communication link and the WiFi interference is different. For example, under 10 Mbps WiFi interference, the PDR of the communication link $L5$ and $L6$ are 63.6% and 54.6%, respectively.

Clearly, we can see that PDR of the communication link reflects the WiFi interference strength. Due to the relationship between the accuracy of RFDL system and PDR (seen in Figure 1), more accurate localization results can be obtained, by assigning higher weights to the communication channels according to the PDR.

As shown in Figure 9, we evaluate the performance of our adaptive weighting RTI. With the increase in the WiFi interference, our adaptive weighting RTI can adjust the usage percentage of each channel, adaptively. For example, because of suffering from different intensity of WiFi interference, the usage ratios of channel 18 is 29.47% in the environment without WiFi interference and drops to 2.63% when the intensity of WiFi interference is 10 Mbps. At the same time, the usage percentages of the other three channels increase accordingly.

We can also see from Figure 9 that the usage ratios of each channel are 37.89% for channel 11, 29.47% for channel 18, 24.74% for channel 21, and 7.89% for channel 26, respectively, in the environment without WiFi interference (0 kbps). According to the work in Kaltioakallio et al.,²³ the aforementioned percentages keep the same, no matter how strong the WiFi interference is in the environment. Due to the reason that no WiFi interference was taken into consideration, the localization accuracy of multi-channel RTI deteriorated severely, from 0.4435 m (without WiFi interference) to 0.990 m (with 10 Mbps WiFi interference), a 123.3% deterioration, as shown in Figure 10.

In addition, we can see that our adaptive weighting RTI model is able to change the usage percentage of each channel according to the intensity of WiFi interference. As shown in Figure 9, channel 18 is not always the best measurement frequency for some communication links because of the WiFi interference. Its usage

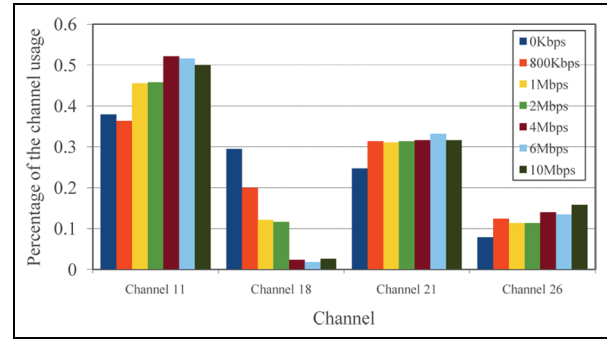


Figure 9. Channel distribution of the IEEE 802.15.4 sensor network under different intensities of WiFi interference.

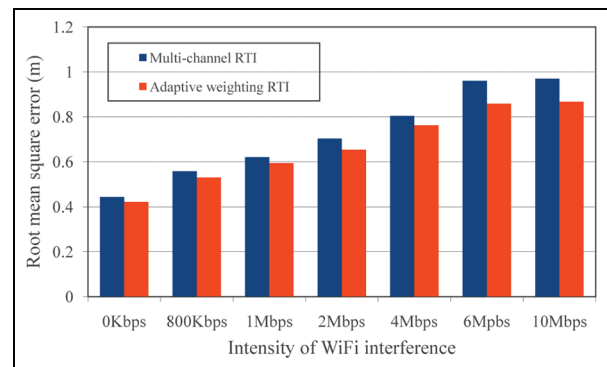


Figure 10. The localization accuracy comparison between the adaptive weighting RTI algorithm and the multi-channel RTI.

ratio changes dynamically according to the WiFi interference. The stronger the WiFi, the smaller the usage ratio. For example, the usage ratios of channel 18 is 29.47% in the environment without WiFi interference and dropped to 1.84% in the environment with 10 Mbps WiFi interference. Accordingly, the usage ratio of channels 11, 21, and 26 increases by 12.11%, 7.90%, and 7.62%, respectively.

As shown in Figure 10, the localization accuracy of the adaptive weighting RTI is 0.5941 m, a 4.51% improvement compared with the multi-channel RTI,²³ in the environment with 1 Mbps WiFi interference. Although the localization accuracy of adaptive weighting RTI also becomes worse with increasing of the WiFi interference, the adaptive weighting RTI outperforms the multi-channel RTI in all WiFi interference scenarios. The reason is that the adaptive weighting RTI can not only dynamically rank the measurement channel for each communication link according to the combination weight (as described in section “Adaptive channel weight model”) but also utilizing the measurement information of all channel by assigning the combination weight.

We also present more detailed views of localization data in Figures 11–13. Figures 11(a) and (b) and 12(a)

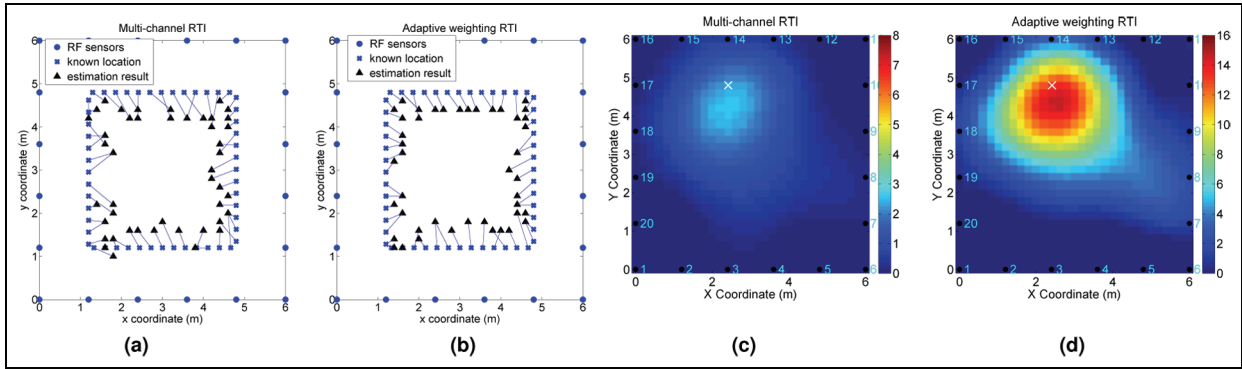


Figure 11. Experiment results in the environment without WiFi interference: (a) channel diversity RTI layout, (b) adaptive weighting RTI layout, (c) multi-channel RTI, and (d) our adaptive weighting RTI.

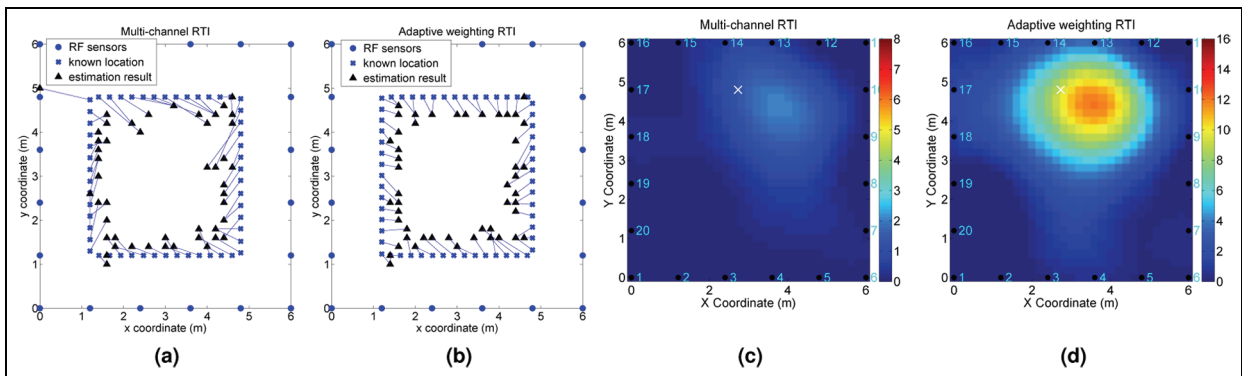


Figure 12. Experiment results in the environment with 2M WiFi interference: (a) channel diversity RTI layout, (b) adaptive weighting RTI layout, (c) channel diversity RTI, and (d) our adaptive weighting RTI.

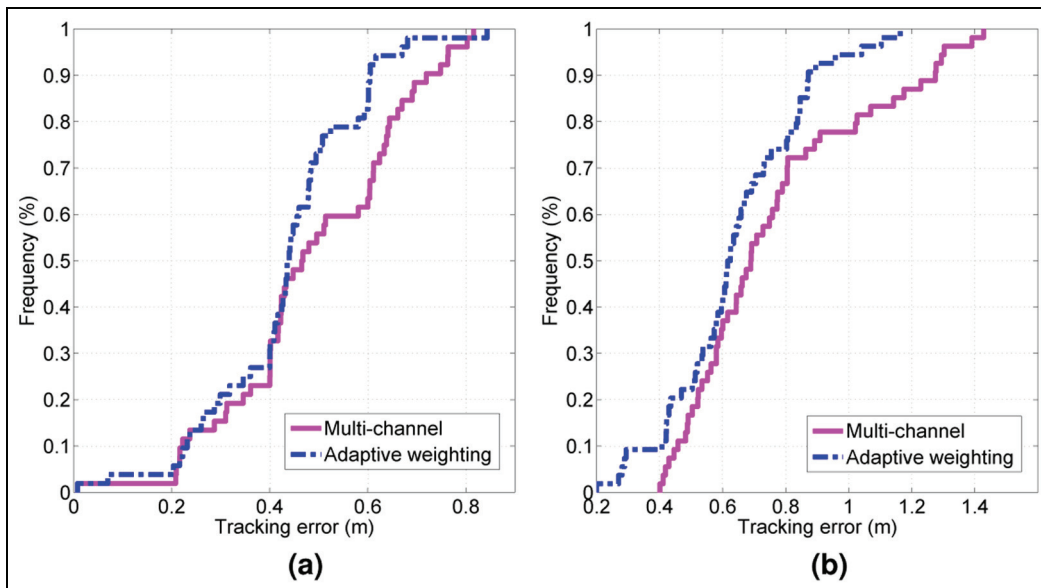


Figure 13. Cumulative distribution functions (CDFs) of localization errors: (a) CDFs in the environment without WiFi interference and (b) CDFs in the environment with 2 Mbps WiFi interference.

and (b) show the relationship between the estimated and the actual localization. In general, the estimation results from adaptive weighting RTI are closer to the known locations than that from multi-channel RTI (seen in Figures 11(a) and (b) and 12(a) and (b)). What's more, radio tomography images from adaptive weighting RTI (seen in Figures 11(d) and 12(d)) also outperform the results in multi-channel RTI (seen in Figures 11(c) and 12(c)), respectively. From the view of the cumulative distribution functions (CDFs), as shown in Figure 13, we can also benefit from the adaptive weighting model. Such as, in the environment with 2 Mbps WiFi interference, for the adaptive weighting model, 95% of localization errors are below 1 m, while 79% of errors from multi-channel are below 1 m, a 16% improvement.

Conclusion

In this article, we introduced an adaptive weighting RTI to improve the accuracy of RTI in the environment with multipath and WiFi interference. In order to locate the target more accurately, we proposed the adaptive weighting RTI method relying on the adaptive channel weight, which is determined by the fade level and the PDR. Extensive experimental results show that our adaptive weighting RTI outperforms the method by channel diversity. In the environment without WiFi interference, there is still an improvement of 4.9%. The stronger the WiFi interference in the multipath environment, the better performance we can obtain from the adaptive weighting RTI (e.g. the improvements of 5.23%, 10.58%, and 12.67%, respectively, in the environment with 4, 6, and 10 Mbps WiFi environment).

Acknowledgements

The authors would like to thank Chih-Ming Hsieh, Sammer Srouji, and Farzad Samie Ghahfarokhi from Chair for Embedded Systems in Department of Computer Science of KIT-Karlsruhe Institute of Technology Germany for their contributions to this work.

Declaration of conflicting interests

The author(s) declared no potential conflicts of interest with respect to the research, authorship, and/or publication of this article.

Funding

The author(s) disclosed receipt of the following financial support for the research, authorship, and/or publication of this article: The authors would like to thank the financial support by Jiangsu Province Science Foundation for Youths (BK20160841) and the financial support of the Fundamental

Research Funds for the Central Universities of China, grant No. 30915118817.

References

1. Sukkariéh S, Nebot EM and Durrant-Whyte HF. A high integrity imu/gps navigation loop for autonomous land vehicle applications. *IEEE T Robot Autom* 1999; 15(3): 572–578.
2. Zhou J and Shi J. Rfid localization algorithms and applications—a review. *J Intell Manuf* 2009; 20(6): 695–707.
3. Patwari N, Ash JN, Kyperountas S, et al. Locating the nodes: cooperative localization in wireless sensor networks. *IEEE Signal Proc Mag* 2005; 22(4): 54–69.
4. Wilson J and Patwari N. Radio tomographic imaging with wireless networks. *IEEE T Mobile Computing* 2010; 9(5): 621–632.
5. Chen X, Edelstein A, Li Y, et al. Sequential Monte Carlo for simultaneous passive device-free tracking and sensor localization using received signal strength measurements. In: *Proceedings of the 10th international conference on information processing in sensor networks (IPSN)*, Chicago, IL, USA, 12–14 April 2011, pp.342–353. New York: IEEE.
6. Seifeldin M, Saeed A, Kosba AE, et al. Nuzzer: a large-scale device-free passive localization system for wireless environments. *IEEE T Mobile Comput* 2013; 12(7): 1321–1334.
7. Mager B, Patwari N and Bocca M. Fall detection using rf sensor networks. In: *Proceedings of the IEEE 24th international symposium on personal indoor and mobile radio communications (PIMRC)*, London, UK, 8–11 September 2013, pp.3472–3476. New York: IEEE.
8. Anderson CR, Martin RK, Walker TO, et al. Radio tomography for roadside surveillance. *IEEE J Sel Top Signa* 2013; 8(1): 66–79.
9. Bocca M, Kaltiokallio O and Patwari N. Radio tomographic imaging for ambient assisted living. In: Chessa S and Knauth S (eds) *Evaluating AAL systems through competitive benchmarking*. Berlin: Springer, 2013, pp.108–130.
10. Patwari N, Brewer L, Tate Q, et al. Breathfinding: a wireless network that monitors and locates breathing in a home. *IEEE J Sel Top Signa* 2013; 8: 30–42.
11. Kaltiokallio O, Bocca M and Patwari N. Follow @grandma: long-term device-free localization for residential monitoring. In: *Proceedings of the IEEE 37th conference on local computer networks workshops (LCN Workshops)*, Sydney, Australia, 22–25 October 2013, pp.991–998. New York: IEEE.
12. Bocca M, Kaltiokallio O, Patwari N, et al. Multiple target tracking with rf sensor networks. *IEEE T Mobile Comput* 2014; 13(8): 1787–1800.
13. Xu C, Firner B, Moore RS, et al. SCPL: indoor device-free multi-subject counting and localization using radio signal strength. In: *Proceedings of the 12th international conference on information processing in sensor networks, Philadelphia, PA*, 8–11 April 2013, pp.79–90. New York: IEEE.
14. Wilson J and Patwari N. See-through walls: motion tracking using variance-based radio tomography networks. *IEEE T Mobile Comput* 2011; 10(5): 612–621.

15. Seinfeldin M and Youssef M. A deterministic large-scale device-free passive localization system for wireless environments. In: *Proceedings of the 3rd international conference on pervasive technologies related to assistive environments*, Samos, 23–25 June 2010, p.51. New York: ACM.
16. Zhao Y, Patwari N, Phillips JM, et al. Radio tomographic imaging and tracking of stationary and moving people via kernel distance. In: *Proceedings of the 12th international conference on information processing in sensor networks*, Philadelphia, PA, 8–11 April 2013, pp.229–240. New York: IEEE.
17. Guo Y, Huang K, Jiang N, et al. An exponential-rayleigh model for rss-based device-free localization and tracking. *IEEE T Mobile Comput* 2015; 14: 484–494.
18. Angrisani L, Bertocco M, Fortin D, et al. Experimental study of coexistence issues between IEEE 802.11 b and IEEE 802.15. 4 wireless networks. *IEEE T Instrum Meas* 2008; 57(8): 1514–1523.
19. Liang CJM, Priyantha NB, Liu J, et al. Surviving wi-fi interference in low power zigbee networks. In: *Proceedings of the 8th ACM conference on embedded networked sensor systems*, Zurich, 3–5 November 2010, pp.309–322. New York: ACM.
20. Manyi W, Zhonglei W, Enjie D, et al. Dual-band sensor network for accurate device-free localization in indoor environment with wifi interference. *IEICE T Inf Syst* 2015; 98(3): 596–606.
21. Xu C, Firner B, Zhang Y, et al. Improving rf-based device-free passive localization in cluttered indoor environments through probabilistic classification methods. In: *Proceedings of the 11th international conference on information processing in sensor networks*, Beijing, China, 16–20 April 2012, pp.209–220. New York: ACM.
22. Moussa M and Youssef M. Smart devices for smart environments: device-free passive detection in real environments. In *Proceedings of the IEEE international conference on pervasive computing and communications (PerCom 2009)*, Galveston, TX, USA, 9–13 March 2009, pp.1–6. New York: IEEE.
23. Kaltiokallio O, Bocca M and Patwari N. Enhancing the accuracy of radio tomographic imaging using channel diversity. In: *Proceedings of the IEEE 9th international conference on mobile ad hoc and sensor systems (MASS)*, Las Vegas, Nevada, USA, 8–11 October 2012, pp.254–262. New York: IEEE.
24. Zhao Y and Patwari N. Noise reduction for variance-based device-free localization and tracking. In: *Proceedings of the 8th annual IEEE communications society conference on sensor, mesh and ad hoc communications and networks (SECON)*, Salt Lake City, Utah, USA, 27–30 June 2011, pp.179–187. New York: IEEE.
25. Kaltiokallio O, Bocca M and Patwari N. *A multi-scale spatial model for rss-based device-free localization*, arXiv preprint arXiv:1302.5914, 2013. (Published online)
26. Lau SY, Lin TH, Huang TY, et al. A measurement study of zigbee-based indoor localization systems under rf interference. In: *Proceedings of the 4th ACM international workshop on experimental evaluation and characterization*, Beijing, China, 21 September 2009, pp.35–42. New York: ACM.
27. Wilson J and Patwari N. A fade-level skew-laplace signal strength model for device-free localization with wireless networks. *IEEE T Mobile Comput* 2012; 11(6): 947–958.
28. IEEE 802.15.4. Standard technical specs, <http://www.ieee802.org/15/pub/TG4Expert.html>
29. Patwari N and Agrawal P. Effects of correlated shadowing: connectivity, localization, and rf tomography. In: *Proceedings of the international conference on information processing in sensor networks (IPSN'08)*, Louis, Missouri, USA, 22–24 April 2008, pp.82–93. New York: IEEE.
30. Agrawal P and Patwari N. Correlated link shadow fading in multi-hop wireless networks. *IEEE T Wirel Commun* 2009; 8(8): 4024–4036.
31. Texas Instruments. A usb-enabled system-on-chip solution for 2.4 GHz IEEE 802.15.4 and zigbee applications, <http://www.ti.com/lit/ds/symlink/cc2531.pdf>
32. Iperf Tool. Iperf was originally developed by nlanr/dast as a modern alternative for measuring tcp and udp bandwidth performance, <https://iperf.fr/>